

Analyses of Inclined Cracks Neighboring Two Iso-Path Cracks in Rock-Like Specimens Under Compression

Abolfazl Abdollahipour  · Mohammad Fatehi Marji

Received: 13 April 2016 / Accepted: 25 September 2016 / Published online: 1 October 2016
© Springer International Publishing Switzerland 2016

Abstract Crack propagation process in pre-cracked rock like specimens has been studied experimentally and numerically considering three cracks in the middle part of each specimen. The rock-like specimens are specially prepared from Portland pozzolana cement, fine sands and water. These pre-cracked cylindrical specimens (each containing a single inclined crack in the neighborhood of two iso-path cracks) are experimentally tested under compressive loading. The same problems are numerically simulated by a modified displacement discontinuity method using higher order displacement discontinuity elements and higher order special crack tip elements for crack tip treatment to increase the accuracy of the Mode I and Mode II stress intensity factors obtained based on linear elastic fracture mechanics theory. The crack propagation and coalescence paths of the inclined crack are estimated by implementing a suitable iteration algorithm of incremental crack length extension in a direction predicted by using the maximum tangential stress criterion. The numerical and analytical crack extension analyses are compared which are in good agreement and show the validity, applicability and accuracy of the present work.

Keywords Inclined crack · Iso-path cracks · Rock-like specimens · Crack propagation · Numerical analyses · Experimental analyses

1 Introduction

The recognition of micro cracks and cracks orientation are of main concern to rock fracture engineers since it contributes to a better understanding and design of geo-mechanical projects. This shows the importance of study of crack propagation and cracks coalescence phenomena in rock materials under various loading conditions. More specifically, the pre-existing cracks and their inclinations have always been considered as vital structures in controlling the strength of brittle materials (Barton 1973).

The pre-existing cracks in rocks are normally under compression and mainly propagate in a stable manner due to formation of wing and/or secondary cracks (Haeri et al. 2013b). It is mainly expected that the crack propagation follows the direction (approximately) parallel to the maximum compressive stress for uniaxial compression case (Hoek and Bieniawski 1965). In a crack propagation process of the brittle solids (such as rock-like specimens) usually two types of cracks are observed which are originating from the original tips of the pre-existing cracks i.e. wing cracks and secondary cracks. Wing cracks are usually produced due to tension while secondary cracks may initiate due to shear. Therefore, it is more likely to

A. Abdollahipour (✉) · M. Fatehi Marji
Faculty of Mining and Metallurgical Engineering,
Yazd University, Yazd 89195-741, Iran
e-mail: a.abdollahipour@yahoo.com

observe wing cracks initiation in rocks since rock have usually lower tension toughness than shear toughness (Bieniawski 1967). Generally, wing cracks are considered as the emanating tensile cracks that initiate at or near the original tips of pre-existing cracks and propagate in a curved path (with increasing load) while the secondary cracks can be considered as shear cracks that may grow from the original tips of the cracks in two different directions, coplanar (quasi-coplanar), and oblique to the pre-existing cracks (Bobet and Einstein 1998).

In some recent experimental and numerical works the fracturing mechanism of brittle rocks has been studied (Park and Bobet 2009; Janeiro and Einstein 2010; Park and Bobet 2010; Lee and Jeon 2011; Yang 2011; Abdollahipour et al. 2013; Haeri et al. 2013a, 2014a, b, c, d; Zhou et al. 2016). For example, Lee and Jeon performed some uniaxial compression tests on three different materials to experimentally analyze the initiation, propagation and coalescence of pre-existing single and double cracks (depends on the type of material) (Lee and Jeon 2011).

Various numerical methods such as finite element method (FEM), boundary element method (BEM), and discrete element method (DEM) have been developed for the simulation of crack propagation in brittle materials (Tang et al. 2001). Natarajan et al. (2010) proposed an XFEM method for stress intensity factor computation and Simpson and Trevelyan developed an enriched BEM and dual BEM to accurately compute the stress intensity factors (Simpson and Trevelyan 2011).

In the classical fracture mechanics, three important crack initiation criteria were proposed to study the crack propagation mechanism of brittle materials; (1) the maximum tangential stress (σ_{θ} -criterion) (2) the maximum energy release rate (G-criterion) and (3) the minimum energy density criterion (S-criterion) (Bobet and Einstein 1998; Vásárhelyi and Bobet 2000). The modified form of the mentioned criteria e.g. F-criterion (a modified energy release rate criterion) was proposed by Shen and Stephansson (1993). The breaking mechanism in brittle materials such as rocks has been modeled by using several computer codes such as: FROCK code (Park 2008), rock failure process analysis (RFPA^{2D}) code (Yang 2011), 2D particle flow code (PFC^{2D}) (Vesga et al. 2008; Lee and Jeon 2011; Manouchehrian et al. 2014). Vesga et al. using PFC^{2D} studied the propagation of open cracks

under uniaxial compression in stiff clay samples. They showed a very good similarity between the numerical results and experimental results on stiff clay samples.

In the present study, the cracks propagation mechanism in cylindrical specimens of rock-like materials (containing either single or double cracks in the central part of the specimen) is being analyzed both experimentally and numerically. The centered single and double cracked cylindrical specimens (prepared from PCC, fine sands and water) tested in a compressive testing apparatus in a rock mechanics laboratory. The propagation and coalescence mechanism of cracks through the specimens and in the bridge area (the area in between the two cracks in the specimens containing double cracks) have been studied. Then some of the experimental works are simulated numerically by a modified higher order displacement discontinuity method (HODDM) and the crack propagation, cracks coalescence and the effect of confining pressure are studied based on linear elastic fracture mechanics (LEFM) principles by computing the Mode I and Mode II stress intensity factors (SIFs).

The experimental results are compared with the corresponding numerical results. There is a very good agreement between the crack propagation and cracks coalescence paths obtained experimentally and numerically which shows the accuracy and validity of the present work. It should be noted that the proposed numerical simulation makes the necessary flexibility in the analysis so that it is readily possible to investigate many different cases. Finally, the proposed HODDM is compared to XFEM which is widely used in fracture mechanics studies. The comparison shows clear advantages HODDM.

2 Pre-cracked Rock-Like Specimens

2.1 Cylindrical Specimens

The pre-cracked rock-like cylindrical specimens with 60 mm diameters and 120 mm lengths are specially prepared by mixing the Portland pozzolana cement (PPC), fine sands and water. The mechanical properties of the un-cracked rock-like specimens are obtained by using laboratory tests following ISRM standards. The mechanical properties used in the present analysis are: compressive strength, $\sigma_c = 28$ MPa; Young's modulus, $E = 15$ GPa, Brazilian

tensile strength, $\sigma_t = 3.81$ MPa; Poisson’s ratio, $\nu = 0.21$.

Some uniaxial compression tests are conducted on the rock-like specimens containing three cracks, named 1, 2 and 3. These cracks are created by inserting three thin steel shims with 10 mm width and 1 mm thickness in molds (before casting the specimens). The uniaxial compressive stress, σ was uniformly applied and the loading rate was kept at 0.5 MPa/s during the tests.

Figure 1 illustrates the geometry and loading condition of a pre-cracked specimen with three cracks. Cracks 1 and 2 (iso-path cracks) have constant orientations of $\alpha = 25^\circ$ or 60° . The third crack is oriented at different angles with respect to the direction of cracks 1 and 2 i.e. at angles $\psi = 0^\circ, 45^\circ, 90^\circ$ and 135° (in a counterclockwise direction) as schematically shown in Fig. 1.

All cracks have length of 10 mm. Figure 2 shows cracks geometries and different orientations of the cracks in cylindrical specimens.

2.2 Brazilian Disk Specimens

The pre-cracked rock-like disc specimens with 100 mm, diameter and 27 mm, thickness are prepared using similar mixture of PPC, fine sands and water as stated above. Therefore, the mechanical properties are the same. Also crack length and thickness are the same as before. The Brazilian disc specimens have three parallel cracks with inclination angles of $\alpha = 45^\circ$. Figure 3 illustrates the Brazilian

disc specimen. The compressive line loading, F was applied and the loading rate was kept at 0.5 KN/s during the tests.

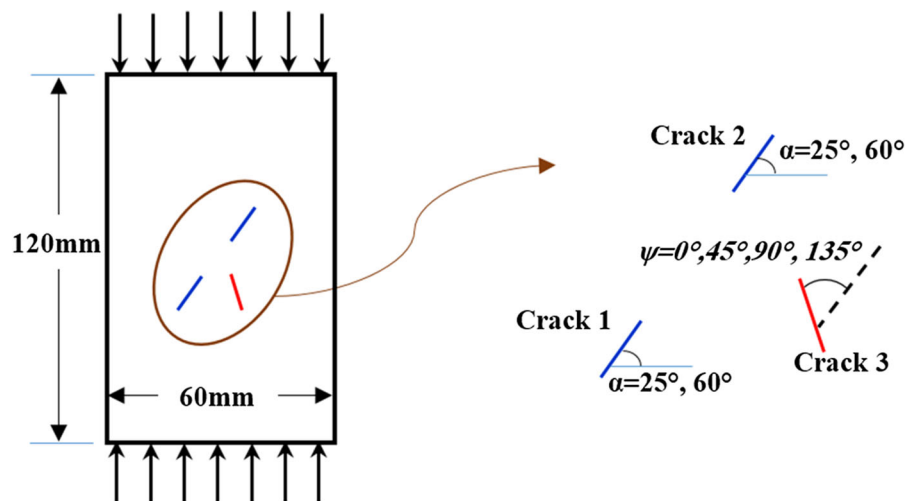
3 Crack Propagation Mechanism (Specimen Testing)

Specimen testing is carried out to obtain the breaking stresses and also to visualize the crack propagation paths and the cracks coalescence in pre-cracked rock-like materials.

3.1 Breaking Stresses of the Pre-cracked Specimens

It has been shown that the pre-cracked rock-like specimens have a lower strength compared to the uncracked specimens (specimens having no cracks) (as it was expected). The breaking stresses of the pre-cracked cylindrical and disk specimens are of paramount importance to study the behavior of the brittle materials. Therefore, the ratios of final breakage stress to the uniaxial compressive strength (σ_F/σ_c) for two cylindrical cases of $\alpha = 25^\circ$ and 60° that the crack 3 is oriented at different angles with respect to the direction of crack 1 and crack 2, $\psi = 0^\circ, 45^\circ, 90^\circ$ and 135° and also a disk specimen containing three parallel cracks of $\alpha = 45^\circ$ are obtained. Results for cylindrical specimens are shown in Fig. 4. The average uniaxial compressive strength of the uncracked specimens is about 28 KN.

Fig. 1 Geometry of the two cracks in a pre-cracked rock-like specimen under uniaxial compression



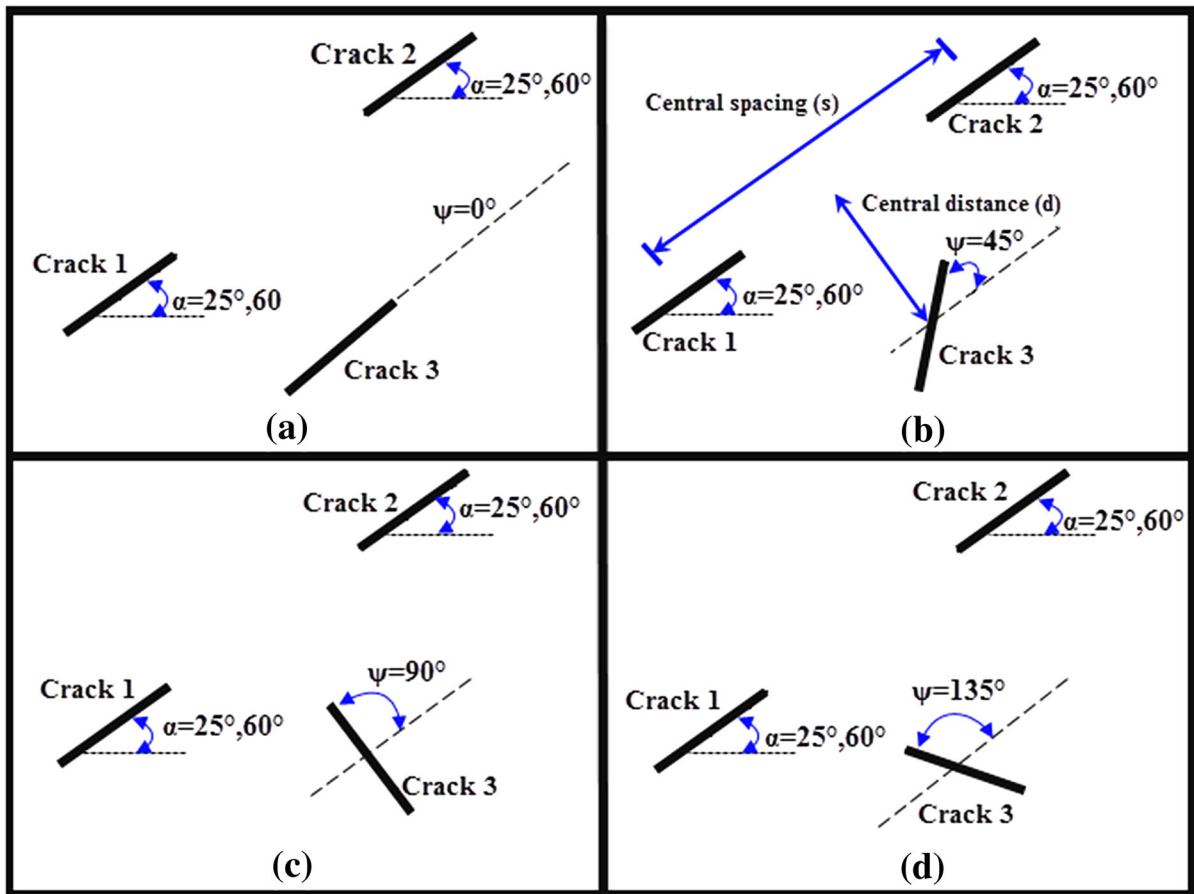


Fig. 2 Crack geometries with spacing $S = 30$ mm in a pre-cracked rock-like specimen with three random cracks, **a** $\psi = 0^\circ$, **b** $\psi = 45^\circ$, **c** $\psi = 90^\circ$, **d** $\psi = 135^\circ$

The ratios of σ_F/σ_c for the cracked specimens are usually less than one (It is 0.33 for disk specimens) because the pre-existing crack decreases the final strength of specimen (Fig. 4). In the cracked cylindrical specimens, breakage stresses at different stages of crack propagation process increases for $\psi = 0^\circ$ to almost 45° but decreases for $\psi = 45^\circ$ – 90° and increases again for $\psi = 90^\circ$ – 135° (Fig. 4). The lowest value of stress is for the case of perpendicular cracks ($\psi = 90^\circ$).

3.2 Crack Propagation Process of Pre-cracked Specimens

Considering a specimen with three cracks in its center the cracks propagation and cracks coalescence phenomena may occur simultaneously because during the test the three pre-existing cracks combine due to propagation of wings and/or secondary cracks for both

cases of cylindrical and disk specimens (originating from the tips of the pre-existing cracks). Figures 5, 6 and 7 show that the cracks coalescence in the bridge area may also occur during the crack propagation process.

The current experiments show that the wing cracks are instantaneously initiated. The development and coalescence of wing cracks in the bridge area may be the main cause of failure in rock-like cylindrical specimens.

It should be noted that for the cases shown in Fig. 5a–c (for $\psi = 0^\circ$, 45° and 90°) the cracks initiated at the tips of all three cracks (crack 1, crack 2 and crack 3) and then the specimen has failed due to the cracks coalescence phenomenon of crack 2 and crack 3. But, for the case of Fig. 5d (for $\psi = 135^\circ$), the wing cracks initiate at the tip of the cracks and the specimen has failed due to cracks coalescence phenomenon of crack 1 and crack 3 (propagated wing

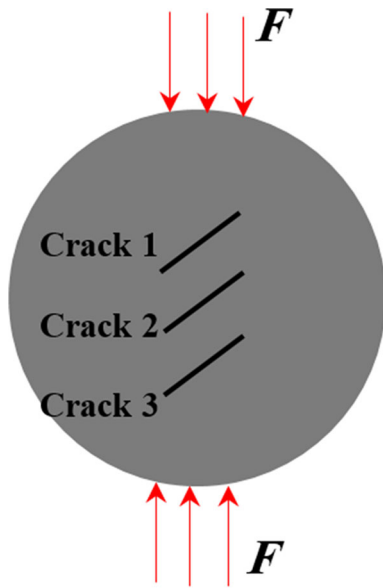


Fig. 3 Geometry of rock-like disc specimens containing three parallel cracks under diametrical compression

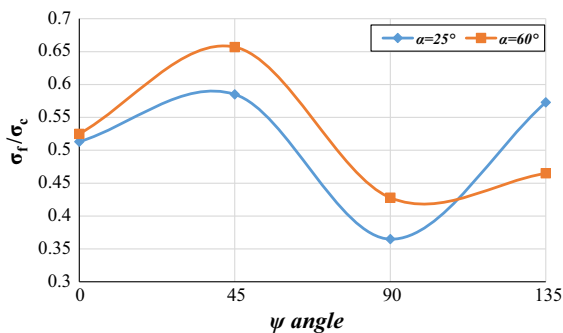


Fig. 4 σ_f/σ_c ratios versus crack inclination angles, $\psi = 0^\circ, 45^\circ, 90^\circ$ and 135° in the three cracked cylindrical specimens for two case crack 1 and crack 2 inclination angle, $\alpha = 25^\circ$ and 60°

crack from the tip of crack 3 is coalesced to the tip of crack 1 and also, no coalescence might occur at the tips of propagating wing cracks). For the case of three parallel cracks in disk specimen (Fig. 6) the crack may or may not propagate from the tips of crack 2 that means the specimen may break due to crack propagation process starting from the tips of crack 1 and crack 3. (i.e. no coalescence might occur at the tips of cracks).

For the case shown in Fig. 7a the wing cracks initiate at the tip of the cracks and propagate in a curved path until propagating wing cracks from crack 2 and crack 3 coalesce with the tip of the crack 1, and

also, no coalescence might occur at the tips of propagating wing cracks. For the cases shown in Fig. 7b–d the bridge area between crack 2 and crack 3 may be considered as the area starting from the upper tip of the crack 3 to that of the lower tip of the crack 2. These cases show the observed wing cracks propagating toward each other and causing cracks coalescence in the bridge area (three cases of coalescence paths is experimentally shown).

4 Indirect Boundary Element Simulation of the Pre-cracked Specimens

The indirect boundary element method implementing the displacement discontinuities along each boundary element in a two dimensional elastostatic body known as displacement discontinuity method (DDM) originally proposed by Crouch (Crouch 1967) is employed to simulate the pre-cracked cylindrical specimens (Marji et al. 2009; Marji and Dehghani 2010; Marji 2013; Haeri et al. 2013a, 2014a, b, c, d) under uniaxial compression.

It has been shown that the higher order displacement discontinuity method (HODDM) gives an accurate solution of normal displacement discontinuity (crack opening displacement) and shear displacement discontinuity (crack sliding displacement) near the crack ends. The Mode I and Mode II SIFs can be formulated based on these discontinuities using the Linear Elastic Fracture Mechanics (LEFM) principles (Irwin 1957). This method gives very accurate results when the special crack tip elements can be used to account for the singularities of stress and displacement fields near the crack ends (Marji et al. 2006). This method also reduces the boundary meshes (elements) as the two sides of the line cracks are simultaneously discretized with similar boundary conditions (Marji et al. 2006).

4.1 Higher Order Displacement Discontinuity Method (HODDM)

Much higher accuracies of the displacement discontinuities along the boundary of the problem can be achieved by using higher order displacement discontinuity (DD) elements (e.g. quadratic or cubic DD elements) in the solution of elastostatic cracked bodies.

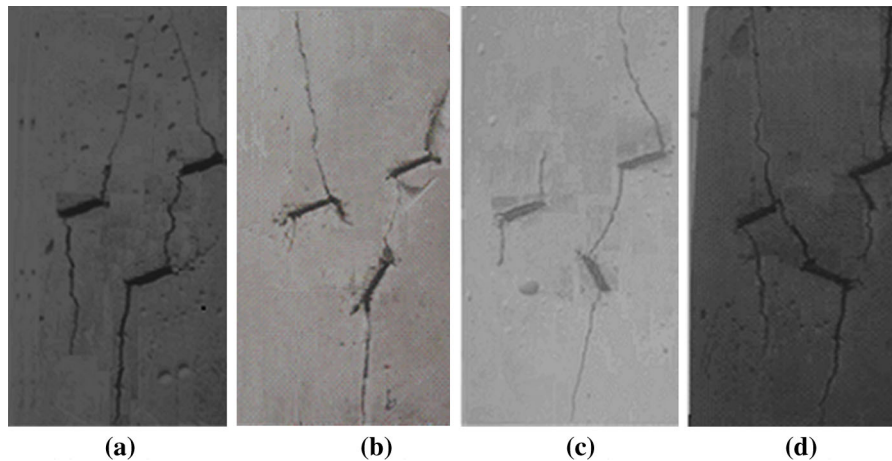


Fig. 5 Experimental results of the coalescence path of rock-like cylindrical specimens containing three cracks under uniaxial compression for case, $\alpha = 25^\circ$ (**a** $\psi = 0^\circ$, **b** $\psi = 45^\circ$, **c** $\psi = 90^\circ$, **d** $\psi = 135^\circ$)



Fig. 6 Experimental results illustrating the breakage path of rock-like disc specimens containing three parallel cracks with constant spacing, $S = 20$ mm

4.1.1 Cubic Element Formulation

A cubic *DD* element $[D_k(\xi)]$ is divided into four equal sub-elements that each sub-element contains a central node for which the nodal *DD* is evaluated numerically (the opening displacement discontinuity D_y and sliding displacement discontinuity D_x) (Marji et al. 2009).

$$D_k(\xi) = \sum_{i=1}^4 N_i(\xi) D_k^i, \quad k = x, y \tag{1}$$

where D_k^1 (i.e. D_x^1 and D_y^1), D_k^2 (i.e. D_x^2 and D_y^2), D_k^3 (i.e. D_x^3 and D_y^3) and D_k^4 (i.e. D_x^4 and D_y^4) are the cubic nodal displacement discontinuities and,

$$\begin{aligned} N_1(\xi) &= -(3a_1^3 - a_1^2\xi - 3a_1\xi^2 + \xi^3)/(48a_1^3), \\ N_2(\xi) &= (9a_1^3 - 9a_1^2\xi - a_1\xi^2 - \xi^3)/(16a_1^3), \\ N_3(\xi) &= (9a_1^3 + 9a_1^2\xi - a_1\xi^2 - \xi^3)/(16a_1^3), \\ N_4(\xi) &= -(3a_1^3 + a_1^2\xi - 3a_1\xi^2 - \xi^3)/(48a_1^3) \end{aligned} \tag{2}$$

are the cubic collocation shape functions using $a_1 = a_2 = a_3 = a_4$. A cubic element is shown in Fig. 8.

The displacements and stresses for a line crack in an infinite body along the x -axis, in terms of single harmonic functions $g(x, y)$ and $f(x, y)$, are (Crouch 1976):

$$\begin{aligned} u_x &= D_x [2(1 - \nu)f_{,y} - yf_{,xx}] + D_y [-(1 - 2\nu)g_{,x} - yg_{,xy}] \\ u_y &= D_x [(1 - 2\nu)f_{,x} - yf_{,xy}] + D_y [2(1 - \nu)g_{,y} - yg_{,yy}] \end{aligned} \tag{3}$$

and the stresses are

$$\begin{aligned} \sigma_{xx} &= 2\mu D_x [2f_{,xy} + yf_{,xyy}] + 2\mu D_y [g_{,yy} + yg_{,yyy}] \\ \sigma_{yy} &= 2\mu D_x [-yf_{,xyy}] + 2\mu D_y [g_{,yy} - yg_{,yyy}] \\ \sigma_{xy} &= 2\mu D_x [2f_{,yy} + yf_{,yyy}] + 2\mu D_y [-yg_{,xyy}] \end{aligned} \tag{4}$$

μ is shear modulus and $f_{,x}, g_{,x}, f_{,y}, g_{,y}$, etc. are the partial derivatives of the single harmonic functions $f(x, y)$ and $g(x, y)$ with respect to x and y , in which these potential functions for the cubic element case can be found from:

$$\begin{aligned} f(x, y) &= \frac{-1}{4\pi(1 - \nu)} \sum_{j=1}^4 D_x^j F_j(I_0, I_1, I_2, I_3) \\ g(x, y) &= \frac{-1}{4\pi(1 - \nu)} \sum_{j=1}^4 D_y^j F_j(I_0, I_1, I_2, I_3) \end{aligned} \tag{5}$$

in which the common function F_j , is defined as

$$F_j(I_0, I_1, I_2, I_3) = \int N_j(\xi) \ln \sqrt{(x - \xi)^2 + y^2} d\xi, \quad j = 1 \text{ to } 4 \tag{6}$$

where the integrals I_0 , to I_3 are expressed as follows:

$$\begin{aligned} I_0(x, y) &= \int_{-a}^a \ln \sqrt{(x - \xi)^2 + y^2} d\xi \\ &= y(\theta_1 - \theta_2) - (x - a) \ln(r_1) + (x + a) \ln(r_2) - 2a \\ I_1(x, y) &= \int_{-a}^a \xi \ln \sqrt{(x - \xi)^2 + y^2} d\xi \\ &= xy(\theta_1 - \theta_2) + 0.5(y^2 - x^2 + a^2) \ln \frac{r_1}{r_2} - ax \\ I_2(x, y) &= \int_{-a}^a \xi^2 \ln \sqrt{(x - \xi)^2 + y^2} d\xi = \frac{y}{3}(3x^2 - y^2) \\ &\quad (\theta_1 - \theta_2) \\ &\quad + \frac{1}{3}(3xy^2 - x^3 + a^3) \ln(r_1) - \frac{1}{3} \\ &\quad (3xy^2 - x^3 - a^3) \ln(r_2) - \frac{2a}{3} \left(x^2 - y^2 + \frac{a^3}{3}\right) \\ I_3(x, y) &= \int_{-a}^a \xi^3 \ln \sqrt{(x - \xi)^2 + y^2} d\xi \\ &= -xy(x^2 - y^2)(\theta_1 - \theta_2) \\ &\quad + 0.25(3x^4 - 6x^2y^2 + 8a^2x^2 + a^4 - y^4) \\ &\quad [\ln(r_1) - \ln(r_2)] - 2ax(x^2 + a^2) \\ &\quad [\ln(r_1) + \ln(r_2)] + 1.5ax^3 - 3axy^2 + 7a^3x/6 \end{aligned} \tag{7}$$

and θ_1, θ_2, r_1 and r_2 are defined as:

$$\begin{aligned} \theta_1 &= \text{tg}^{-1}\left(\frac{y}{x - a}\right), \quad \theta_2 = \text{tg}^{-1}\left(\frac{y}{x + a}\right), \\ r_1 &= \sqrt{(x - a)^2 + y^2}, \quad \text{and} \quad r_2 = \sqrt{(x + a)^2 + y^2} \end{aligned} \tag{8}$$

The partial derivatives of I_3 which are used to calculate displacement discontinuities are provided in ‘‘Appendix 1’’ section. I_0, I_1 and I_2 are completely explained by the second author in (Marji et al. 2006).

4.1.2 Special Crack Tip Element

Since the singularities of the stresses and displacements near the crack ends may reduce their accuracies, special crack tip elements are used to increase the accuracy of the *DDs* near the crack tips (Marji et al. 2006). As shown in Fig. 9, the *DD* variation for four nodes can be formulated using a special crack tip element containing four nodes (or having four special crack tip sub-elements).

$$D_{Ci}(\xi) = [N_{C1}(\xi)]D_{Ci}^1(a) + [N_{C2}(\xi)]D_{Ci}^2(a) + [N_{C3}(\xi)]D_{Ci}^3(a) + [N_{C4}(\xi)]D_{Ci}^4(a) \tag{9}$$

where the crack tip element has a length $a_1 = a_2 = a_3 = a_4$.

Considering a crack tip element with four equal sub-elements ($a_1 = a_2 = a_3 = a_4$), the shape functions $N_{C1}(\xi)$ to $N_{C4}(\xi)$ can be obtained as equations:

$$\begin{aligned} N_{C1}(\xi) &= 2.1336 \left(\frac{\xi}{a_1}\right)^{\frac{1}{2}} - 1.3965 \left(\frac{\xi}{a_1}\right)^{\frac{3}{2}} \\ &\quad + 0.2759 \left(\frac{\xi}{a_1}\right)^{\frac{5}{2}} - 0.0172 \left(\frac{\xi}{a_1}\right)^{\frac{7}{2}} \\ N_{C2}(\xi) &= -0.9475 \left(\frac{\xi}{a_2}\right)^{\frac{1}{2}} + 1.2094 \left(\frac{\xi}{a_2}\right)^{\frac{3}{2}} \\ &\quad - 0.2787 \left(\frac{\xi}{a_2}\right)^{\frac{5}{2}} + 0.0194 \left(\frac{\xi}{a_2}\right)^{\frac{7}{2}} \\ N_{C3}(\xi) &= 0.1908 \left(\frac{\xi}{a_3}\right)^{\frac{1}{2}} - 0.2467 \left(\frac{\xi}{a_3}\right)^{\frac{3}{2}} \\ &\quad + 0.0771 \left(\frac{\xi}{a_3}\right)^{\frac{5}{2}} - 0.0231 \left(\frac{\xi}{a_3}\right)^{\frac{7}{2}} \\ N_{C4}(\xi) &= -0.0977 \left(\frac{\xi}{a_4}\right)^{\frac{1}{2}} + 0.150 \left(\frac{\xi}{a_4}\right)^{\frac{3}{2}} \\ &\quad - 0.0586 \left(\frac{\xi}{a_4}\right)^{\frac{5}{2}} + 0.0065 \left(\frac{\xi}{a_4}\right)^{\frac{7}{2}} \end{aligned} \tag{10}$$

By substituting Eqs. (10) into Eqs. (9) and then substituting these equations into Eqs. (3) and (4) and following the procedures similar to those given for the derivation of the general potential function $F_j(I_0, I_1, I_2, I_3)$ in Eq. (6) the general potential function $f_C(x, y)$ for the crack tip element can be expressed as:

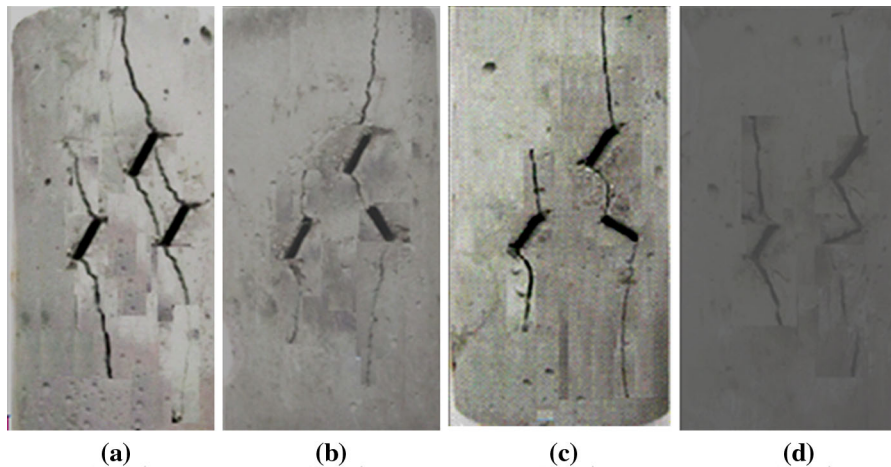


Fig. 7 Experimental results of the coalescence path of rock-like cylindrical specimens containing three cracks under uniaxial compression for case, $\alpha = 60^\circ$ (a $\psi = 0^\circ$, b $\psi = 45^\circ$, c $\psi = 90^\circ$, d $\psi = 135^\circ$)

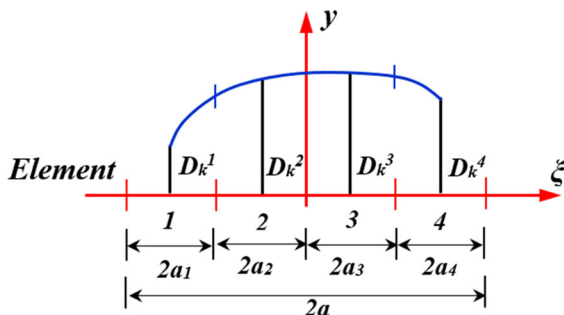


Fig. 8 Cubic collocations for the higher order displacement discontinuity variation

$$\begin{aligned}
 F(x, y) = & -\frac{1}{4\pi(1-\nu)} \left\{ \left[\int_{-a}^a N_{C1}(\xi) \sqrt{(x-\xi)^2 + y^2} d\xi D_i^1 \right] \right. \\
 & + \left[\int_{-a}^a N_{C2}(\xi) \sqrt{(x-\xi)^2 + y^2} d\xi D_i^2 \right] \\
 & + \left[\int_{-a}^a N_{C3}(\xi) \sqrt{(x-\xi)^2 + y^2} d\xi D_i^3 \right] \\
 & \left. \times \left[\int_{-a}^a N_{C4}(\xi) [(x-\xi)^2 + y^2]^{0.5} d\xi D_i^4 \right] \right\} \quad (11)
 \end{aligned}$$

The potential function $F_{Cj}(I_{CK})$ for special crack tip elements can be written in the following form

$$F_C(I_{Cj}) = \int_{-a}^a N_{Cj}(\xi) \ln \sqrt{(x-\xi)^2 + y^2} d\xi \quad (12)$$

And from this, the following integrals are deduced:

$$\begin{aligned}
 I_{C1}(x, y) &= \int_{-a}^a \xi^{\frac{1}{2}} \ln \sqrt{(x-\xi)^2 + y^2} d\xi, \\
 I_{C2}(x, y) &= \int_{-a}^a \xi^{\frac{3}{2}} \ln \sqrt{(x-\xi)^2 + y^2} d\xi \\
 I_{C3}(x, y) &= \int_{-a}^a \xi^{\frac{5}{2}} \ln \sqrt{(x-\xi)^2 + y^2} d\xi, \\
 I_{C4}(x, y) &= \int_{-a}^a \xi^{\frac{7}{2}} \ln \sqrt{(x-\xi)^2 + y^2} d\xi
 \end{aligned} \quad (13)$$

Following the procedure explained by (Marji et al. 2006) the complete solution of the integrals given in Eq. (13) are presented in “Appendix 2” section. It should be noted that for this case also two degrees of freedom are used for each node (boundary collocation points) at the center of each sub-elements. Based on the linear elastic fracture mechanics (LEFM) principles, the Mode I and Mode II stress intensity factors K_I and K_{II} can be easily deduced (Sanford 2003; Marji et al. 2006). A crack tip element of length $2a$ is considered then the stress intensity factors with respect to the normal and shear displacement discontinuities (assuming plane strain condition), can be determined (Shou and Crouch 1995) as:

Fig. 9 A special crack tip element with four equal sub-elements

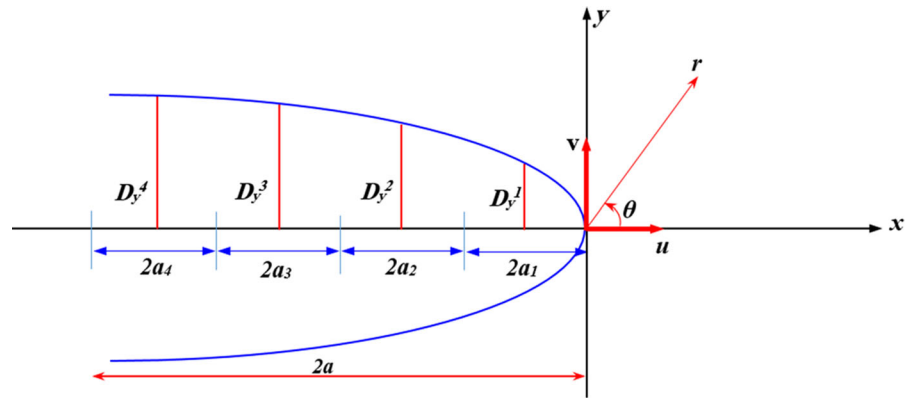
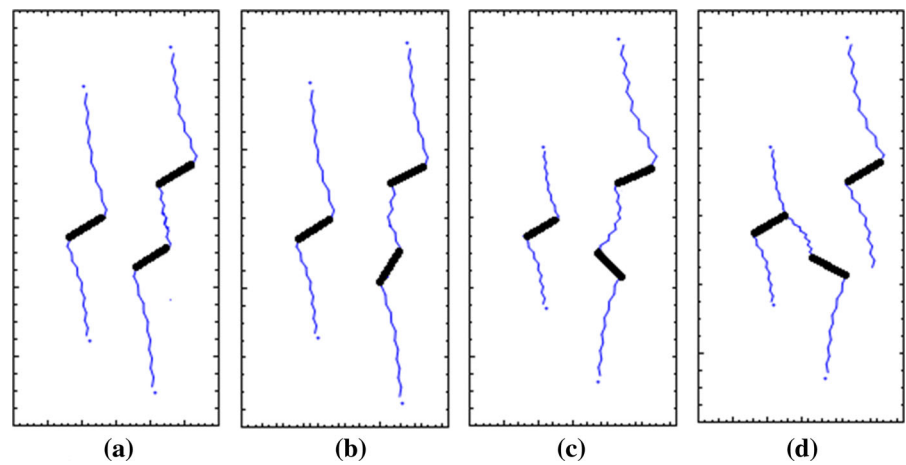


Fig. 10 Numerical simulation of the crack propagation path for cylindrical specimens (with three cracks) under uniaxial compression, **a** $\psi = 0^\circ$, **b** $\psi = 45^\circ$, **c** $\psi = 90^\circ$, **d** $\psi = 135^\circ$



$$K_I = \frac{\mu}{4(1-\nu)} \left(\frac{2\pi}{a}\right)^{\frac{1}{2}} D_y(a), \quad \text{and}$$

$$K_{II} = \frac{\mu}{4(1-\nu)} \left(\frac{2\pi}{a}\right)^{\frac{1}{2}} D_x(a) \quad (14)$$

where μ is the shear modulus and ν is Poisson’s ratio of the brittle material.

4.2 Numerical Simulation of the Pre-cracked Specimens

In this study, a modified higher order displacement discontinuity method is used for the numerical simulation of the proposed experimental work. The cracks propagation and cracks coalescence in the bridge area of rock-like brittle materials is numerically studied and these results are compared with the corresponding results observed experimentally in Figs. 5a–d, 6 and 7a–d.

The cylindrical specimens containing three cracks (already shown in Fig. 5a–d) are simulated by the displacement discontinuity method and the crack propagation paths are graphically shown in Fig. 10a–e. The specimen containing three parallel cracks (already shown in Fig. 6) are simulated by the displacement discontinuity method and the crack propagation paths are graphically shown in Fig. 11. The three different specimens containing three cracks (already shown in Fig. 7a–d) are also simulated by the proposed numerical method and the results are graphically shown in Fig. 12a–d. In the present numerical simulations, the Mode I and Mode II stress intensity factors (SIFs) proposed by Irwin (Irwin 1957) are estimated based on LEFM approach. A boundary element code is provided using the maximum tangential stress criterion given by Erdogan and Sih (Erdogan and Sih 1963) in a stepwise procedure so that the propagation paths of the propagating wing cracks are

estimated (Haeri et al. 2013c). These simulated propagation paths are in good agreement with the corresponding experimental results and are presented in Figs. 10, 11 and 12 for comparison.

4.3 Comparison of HODDM with XFEM

A center horizontal crack with half crack length of $a = 1$ m is used to compare the HODDM with an XFEM method proposed by Natarajan et al. (2010). They used Schwarz–Christoffel conformal mapping (SC Map) for numerical integration. Figure 13 shows

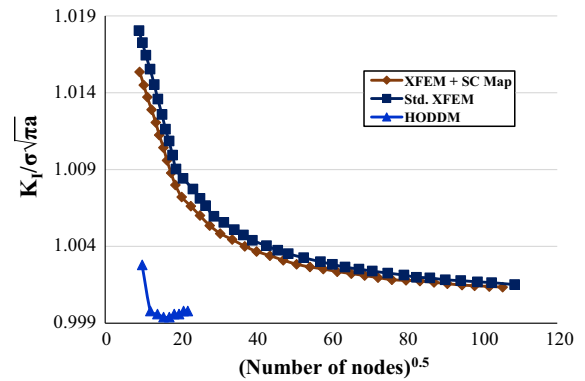


Fig. 13 Comparison of the normalized stress intensity factor, $K_I/(\sigma\sqrt{\pi a})$, for the center crack problem [obtained by the proposed HODDM and XFEM methods given by (Natarajan et al. 2010)]

the results of the current DDM, standard XFEM, and XFEM + SC Map proposed by (Natarajan et al. 2010). They succeeded in improving the accuracy of XFEM, however, their accuracy is still not comparable with the accuracy of DDM used in this study. Using only a small number of elements in the proposed method compared to the XFEM methods a much more accurate result has been obtained.

5 Conclusion

The subject of cracks propagation and cracks coalescence in brittle solids such as geomaterials have found much attention in recent years. As it is a complicated

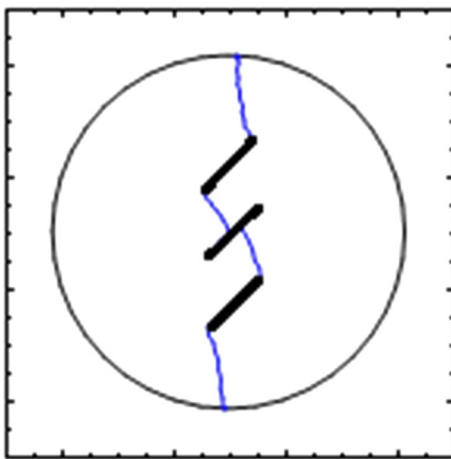
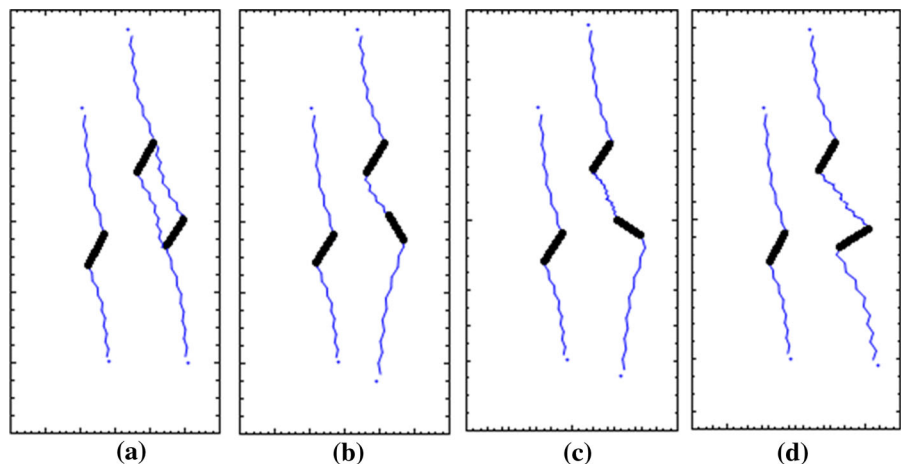


Fig. 11 Numerical simulation of the crack propagation path for pre-cracked Brazilian disc specimen containing three parallel cracks with constant spacing, $S = 20$ mm

Fig. 12 Numerical simulation of crack propagation paths and cracks coalescence for cylindrical specimens (with three cracks) under uniaxial compression, **a** $\psi = 0^\circ$, **b** $\psi = 45^\circ$, **c** $\psi = 90^\circ$, **d** $\psi = 135^\circ$



process further research may be devoted to investigate the crack propagation, cracks coalescence in the bridge area and final breakage paths of the rocks and rock-like materials under uniaxial and biaxial compression. A detailed analysis of the fracturing process of the pre-cracked rock-like cylindrical specimens has been simultaneously accomplished by experimental tests and numerical simulation. Effects of fracturing on the breaking stress of the pre-cracked rock-like materials have been investigated. It has been shown that the crack propagation mechanism in the brittle substances due to the cracks coalescence phenomenon in the bridge area occur mainly by propagation of wing cracks emanating from the tips of the pre-existing cracks. The same experimental specimens are modeled numerically by an indirect boundary element method and the corresponding numerical results are in good agreement with the experimental results. The experimental and numerical models both illustrate the production of the wing cracks and the cracks propagation paths produced by the coalescence phenomenon of the three pre-existing cracks in the bridge area. Therefore, the propagating directions of the wing cracks are changing and inclines toward those of wing cracks propagating under uniaxial compression.

Comparison of the HODDM with XFEM showed that HODDM needs substantially fewer elements for reaching the same level of accuracy as XFEM.

Appendix 1

Cubic integral I_3 , and its derivatives

$$I_3(x, y) = \int_{-a}^a \xi^3 \ln \sqrt{(x - \xi)^2 + y^2} d\xi = -xy(x^2 - y^2)(\theta_1 - \theta_2) + 0.25(3x^4 - 6x^2y^2 + 8a^2x^2 + a^4 - y^4)[\ln(r_1) - \ln(r_2)] - 2ax(x^2 + a^2)[\ln(r_1) + \ln(r_2)] + 1.5ax^3 - 3axy^2 + 7a^3x/6$$

Let, $A_1 = -xy(x^2 - y^2)$, $A_2 = 0.25(3x^4 - 6x^2y^2 + 8a^2x^2 + a^4 - y^4)$, $A_3 = -2ax(x^2 + a^2)$, $A_4 = 1.5ax^3 - 3axy^2 + 7a^3x/6$ and $L_x = [\ln(r_1) + \ln(r_2)]$.

Therefore,

$$\begin{aligned} A_{1,x} &= -3x^2y + y^3, & A_{1,y} &= -x^3 + 3xy^2, \\ A_{x,y} &= -3x^2 + 3y^2, \\ A_{1,yy} &= 6xy, & A_{1,xyy} &= 6y, & A_{1,yyy} &= 6x \\ A_{2,x} &= 3x^3 - 3xy^2 + 4a^2x, & A_{2,y} &= -(3x^2y + y^3), \\ A_{2,xy} &= -6xy, \\ A_{2,yy} &= -3(x^2 + y^2), & A_{2,xyy} &= -6x, & A_{2,yyy} &= -6y, \\ A_{3,x} &= -6ax^2 - 2a^3, & A_{3,y} &= 0, \\ A_{4,x} &= 4.5ax^3 - 3ay^2 + 7a^3/6, \\ A_{4,y} &= -6axy, & A_{4,xy} &= 6ay, & A_{4,yy} &= -6ax, \\ A_{4,xyy} &= -6a, & A_{4,yyy} &= 0 \\ L_{x,x} &= -\left(\frac{(x-a)}{r_1^2} + \frac{(x+a)}{r_2^2}\right), & L_{x,y} &= -\left(\frac{y}{r_1^2} + \frac{y}{r_2^2}\right), \\ L_{x,xy} &= 2y\left(\frac{(x-a)}{r_1^4} + \frac{(x+a)}{r_2^4}\right) \\ L_{x,yy} &= -\left(\frac{(x-a)^2 - y^2}{r_1^4} + \frac{(x+a)^2 - y^2}{r_2^4}\right) \\ L_{x,yyy} &= -2\left(\frac{(x-a)(r_1^2 - 4y^2)}{r_1^6} + \frac{(x+a)(r_2^2 - 4y^2)}{r_2^6}\right) \\ L_{x,xyy} &= -2y\left(\frac{3(x-a)^2 - y^2}{r_1^6} + \frac{3(x+a)^2 - y^2}{r_2^6}\right) \\ I_3(x, y) &= A_1I_{0,y} + A_2I_{0,x} + A_3L_x + A_4 \\ I_{3,x} &= A_{1,x}I_{0,y} + A_1I_{0,xy} + A_{2,x}I_{0,x} + A_2I_{0,xx} + A_{3,x}L_x \\ &\quad + A_3L_{x,x} + A_{4,x} \\ I_{3,y} &= A_{1,y}I_{0,y} + A_1I_{0,yy} + A_{2,y}I_{0,x} + A_2I_{0,xy} + A_3L_{x,y} \\ &\quad + A_{4,y} \\ I_{3,xy} &= A_{1,xy}I_{0,y} + A_{2,xy}I_{0,x} + (A_{1,y} + A_{2,x})I_{0,xy} \\ &\quad + (A_{1,x} - A_{2,y})I_{0,yy} \\ &\quad + A_1I_{0,xyy} - A_2I_{0,yyy} + A_{3,x}L_{x,y} + A_3L_{x,xy} + A_{4,xy} \\ I_{3,yy} &= A_{1,yy}I_{0,y} + A_{2,yy}I_{0,x} + 2A_{1,y}I_{0,yy} \\ &\quad + 2A_{2,y}I_{0,xy} + A_1I_{0,yyy} + A_3L_{yy} - 6ax \\ I_{3,xyy} &= A_{1,xyy}I_{0,y} + A_{2,xyy}I_{0,x} + (A_{1,yy} + 2A_{2,xy})I_{0,xy} \\ &\quad + (2A_{1,xy} - A_{2,yy})I_{0,yy} + (2A_{1,y} + A_{2,x})I_{0,xyy} \\ &\quad + A_{1,x} - 2A_{2,y}A_2I_{0,yyy} \\ &\quad + A_1I_{0,xyyy} - A_2I_{0,yyyy} + A_{3,x}L_{yy} + A_3L_{xyy} + A_{4,xyy} \\ I_{3,yyy} &= 6xI_{0,y} - 6yI_{0,x} + 18xyI_{0,yy} - 9(x^2 + y^2)I_{0,xy} \\ &\quad \times 2A_{2,y}I_{0,xyy} + 3A_{1,y}I_{0,yyy} + A_1I_{0,yyyy} + A_3L_{x,yyy} \end{aligned}$$

Appendix 2

Special singular integral i_{c4} and its derivatives

$$I_{C4}(x, y) = \int_0^{2a} \xi^{\frac{7}{2}} \ln \sqrt{(x - \xi)^2 + y^2} d\xi$$

$$= \frac{32\sqrt{2}}{9} a^{\frac{9}{2}} \ln \sqrt{(x - 2a)^2 + y^2} + \frac{2x}{9} F_1 - \frac{2}{9} F_2$$

where

$$F_1 = \int_0^{2a} \frac{\xi^{\frac{9}{2}} d\xi}{[(x - \xi)^2 + y^2]} = -\frac{2}{7} (2a)^{3.5} - \frac{4x}{5} (2a)^{2.5}$$

$$- 2 \left(x^2 - \frac{y^2}{3} \right) (2a)^{1.5} - (x^2 + y^2) (3x^2 - y^2) G_1$$

$$+ 4x(x^2 - y^2) G_2$$

$$F_2 = \int_0^{2a} \frac{\xi^{\frac{11}{2}}}{\left[\left[(x - \xi)^2 + y^2 \right] \right]} d\xi = -\frac{2}{9} (2a)^{4.5}$$

$$- \frac{4x}{7} (2a)^{3.5} - \frac{2}{5} (3x^2 - y^2) (2a)^{2.5}$$

$$- \frac{8x}{3} (x^2 - y^2) (2a)^{1.5} - 2x(x^4 - y^4) G_1$$

$$+ (5x^4 - 10x^2y^2 + y^4) G_2$$

and G_1 and G_2 are:

$$G_1 = \int_0^{2a} \frac{\xi^{\frac{1}{2}}}{[(x - \xi)^2 + y^2]} d\xi$$

$$= \rho^{-1} \left[0.5 \left(\cos \phi - \left(\frac{x}{y} \right) \sin \phi \right) \ln \frac{2a - 2\sqrt{2a}\rho \cos \phi + \rho^2}{2a + 2\sqrt{2a}\rho \cos \phi + \rho^2} \right.$$

$$\left. + \left(\sin \phi + \left(\frac{x}{y} \right) \cos \phi \right) \times \operatorname{tg}^{-1} \left(\frac{2\sqrt{2a}\rho \sin \phi}{\rho^2 - 2a} \right) \right]$$

$$G_2 = \int_0^{2a} \frac{\xi^{\frac{3}{2}}}{\left[\left[(x - \xi)^2 + y^2 \right] \right]} d\xi$$

$$= -2(2a)^{0.5} + \frac{x^2 - y^2}{2y} \operatorname{tg}^{-1} \left(\frac{x - 2a}{y} \right) - 2xG_1$$

References

- Abdollahipour A, Marji MF, Yarahmadi-Bafghi AR (2013) A fracture mechanics concept of in situ stress measurement by hydraulic fracturing test. In: The 6th international symposium on in-situ rock stress, ISRM, Sendai
- Barton N (1973) Review of a new shear-strength criterion for rock joints. *Eng Geol* 7:287–332
- Bieniawski ZT (1967) Mechanics of brittle fracture of rocks, part I, II and III. *Int J Rock Mech Min Sci Geomech Abstr* 4:395–430
- Bobet A, Einstein HH (1998) Fracture coalescence in rock-type materials under uniaxial and biaxial compression. *Int J Rock Mech Min Sci* 35:863–888
- Crouch S (1967) Analysis of stresses and displacements around underground excavations: an application of the displacement discontinuity method. Minneapolis
- Crouch SL (1976) Solution of plane elasticity problems by the displacement discontinuity method. I. Infinite body solution. *Int J Numer Methods Eng* 10:301–343
- Erdogan F, Sih G (1963) On the crack extension in plates under loading and transverse shear. *J Basic Eng* 85:519–527
- Haeri H, Shahriar K, Marji MF et al (2013a) Modeling the propagation mechanism of two random micro cracks in rock samples under uniform tensile loading. In: 13th international conference on fracture, Beijing
- Haeri H, Shahriar K, Marji MF, Moarefvand P (2013b) A coupled numerical-experimental study of the breakage process of brittle substances. *Arabi J Geosci* 8(2):809–825
- Haeri H, Shahriar K, Marji MF, Moarefvand P (2013c) On the crack propagation analysis of rock like Brazilian disc specimens containing cracks under compressive line loading. *Lat Am J Solids Struc* 11(8):400–416
- Haeri H, Shahriar K, Marji MF, Moarefvand P (2014a) On the cracks coalescence mechanism and cracks propagation paths in rock-like specimens containing pre-existing random cracks under compression. *J Cent South Univ* 21(16):2404–2414
- Haeri H, Shahriar K, Marji MF, Moarefvand P (2014b) Investigating the fracturing process of rock-like Brazilian discs containing three parallel cracks under compressive line loading. *Strength Mater* 46(3):404–416
- Haeri H, Shahriar K, Marji MF, Moarefvand P (2014c) A boundary element analysis of the crack propagation mechanism of random micro cracks in rock-like specimens under uniform normal tension. *J Min Environ Eng* 6(1):73–93
- Haeri H, Shahriar K, Marji MF, Moarefvand P (2014d) On the strength and crack propagation process of the pre-cracked rock-like specimens under uniaxial compression. *Strength Mater* 46(1):140–152
- Hoek E, Bieniawski ZT (1965) Brittle rock fracture propagation. *Rock Under Compress Brittle Rock Fract Propag Rock Under Compress* 1:137–155
- Irwin GR (1957) Analysis of stresses and strains near the end of a crack. *J Appl Mech* 24:361
- Janeiro RP, Einstein HH (2010) Experimental study of the cracking behavior of specimens containing inclusions (under uniaxial compression). *Int J Fract* 164:83–102
- Lee H, Jeon S (2011) An experimental and numerical study of fracture coalescence in pre-cracked specimens under uniaxial compression. *Int J Solids Struct* 48:979–999
- Manouchehrian A, Sharifzadeh M, Marji MF, Gholamnejad J (2014) A bonded particle model for analysis of the flaw orientation effect on crack propagation mechanism in brittle materials under compression. *Arch Civ Mech Eng* 14:40–52
- Marji MF (2013) On the use of power series solution method in the crack analysis of brittle materials by indirect boundary element method. *Eng Fract Mech* 98:365–382

- Marji MF, Dehghani I (2010) Kinked crack analysis by a hybridized boundary element/boundary collocation method. *Int J Solids Struct* 47:922–933. doi:[10.1016/j.ijsolstr.2009.12.008](https://doi.org/10.1016/j.ijsolstr.2009.12.008)
- Marji MF, Hosseini Nasab H, Kohsary AH (2006) On the uses of special crack tip elements in numerical rock fracture mechanics. *Int J Solids Struct* 43:1669–1692. doi:[10.1016/j.ijsolstr.2005.04.042](https://doi.org/10.1016/j.ijsolstr.2005.04.042)
- Marji MF, Hosseini-Nasab H, Morshedi AH (2009) Numerical modeling of the mechanism of crack propagation in rocks under TBM disc cutters. *Mech Mater Struct* 4:605–627
- Natarajan S, Mahapatra DR, Bordas SPA (2010) Integrating strong and weak discontinuities without integration sub-cells and example applications in an XFEM/GFEM framework. *Int J Numer Meth Eng* 83:269–294
- Park CH (2008) Coalescence of frictional fractures in rock materials. Purdue University, West Lafayette
- Park C, Bobet A (2009) Crack coalescence in specimens with open and closed flaws. *Int J Rock Mech Min Sci* 46:819–829
- Park CH, Bobet A (2010) Crack initiation, propagation and coalescence from frictional flaws in uniaxial compression. *Eng Fract Mech* 77:2727–2748
- Sanford RJ (2003) Principles of fracture mechanics. Prentice Hall, Upper Saddle River
- Shen B, Stephansson O (1993) Modification of the G-criterion of crack propagation in compression. *Int J Eng Fract Mech* 47:177–189
- Shou KJ, Crouch SL (1995) A higher order displacement discontinuity method for analysis of crack problems. *Int J Rock Mech Min Sci Geomech Abstr* 32:49–55
- Simpson R, Trevelyan J (2011) A partition of unity enriched dual boundary element method for accurate computations in fracture mechanics. *Comput Methods Appl Mech Eng* 200:1–10
- Tang CA, Lin P, Wong RHC, Ai E (2001) Analysis of crack coalescence in rock-like materials containing three flaws—part II: numerical approach. *Int J Rock Mech Min Sci* 38:925–939
- Vásárhelyi B, Bobet A (2000) Modeling of crack initiation, propagation and coalescence in uniaxial compression. *Rock Mech Rock Eng* 33(2):119–139
- Vesga LF, Vallejo LE, Lobo-Guerrero S (2008) DEM analysis of the crack propagation in brittle clays under uniaxial compression tests. *Int J Numer Anal methods Geomech* 32:1405–1415
- Yang S (2011) Crack coalescence behavior of brittle sandstone samples containing two coplanar fissures in the process of deformation failure. *Eng Fract Mech* 78:3059–3081
- Zhou Z, Abass H, Li X, Teklu T (2016) Experimental investigation of the effect of imbibition on shale permeability during hydraulic fracturing. *J Nat Gas Sci Eng*. doi:[10.1016/j.jngse.2016.01.023](https://doi.org/10.1016/j.jngse.2016.01.023)